UNCLASSIFIED

THE PENNSYLVANIA STATE UNIVERSITY
INSTITUTE FOR SCIENCE & ENGINEERING
UNIVERSITY PARK, PENNSYLVANIA

An Acoustic-Array Model for the Computation of the Rotational Noise of a Lifting Rotor

Distribution of this document is unlimited.

February 1, 1971

SERIAL NO. TR-1-71

Copy No. 32

NAVY DEPARTMENT-NAVAL ORDNANCE SYSTEMS COMMAND
CONTRACT N00017-70-C-1407

UNCLASSIFIED

Please do not return this document
to the Ordnance Research Laboratory

Destroy it in accordance with the
appropriate security regulations
when it is no longer needed

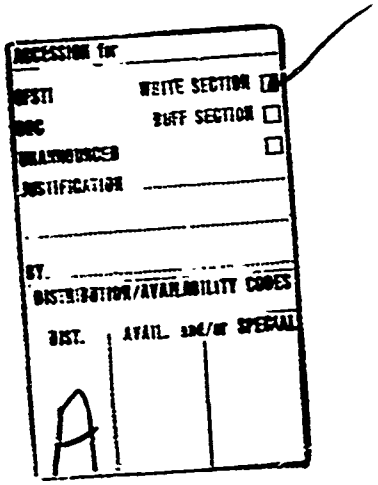

An Acoustic-Array Model for the Computation of the Rotational Noise of a Lifting Rotor

By John A. Macaluso

APPROVED FOR DISTRIBUTION

M. T. Pigott

ASSISTANT DIRECTOR

APPROVED FOR DISTRIBUTION

John C. Johnson

DIRECTOR

14. KEY WORDS	LINK A		LINK B		LINK C	
	ROLE	WT	ROLE	WT	ROLE	WT
Circular Array	8					
Computer program	8					
Helicopter noise	8					
Mathematical Model	8					
Radiated Noise	8					
Rotor Noise	8					
Sound Patterns	8					
Sound Pressure	8					

DOCUMENT CONTROL DATA - R & D

(Security classification of title, abstract and indexing annotation when overall report is classified)

1. ORIGINATING ACTIVITY (Corporate author)	2a. REPORT SECURITY CLASSIFICATION
Ordnance Research Laboratory University Park, Pennsylvania	UNCLASSIFIED 2b. GROUP -------

3. REPORT TITLE

An Acoustic-Array Model for the Computation of the Rotational Noise of a Lifting Rotor

4. DESCRIPTIVE NOTES (Type of report and inclusive dates)

ORL External Report, February 1, 1971

5. AUTHOR(S) (First name, middle initial, last name)

John A. Macaluso

6. REPORT DATE	7a. TOTAL NO. OF PAGES	7b. NO. OF REFS
February 1, 1971	25 pp. & figs.	13

8a. CONTRACT OR GRANT NO.	9a. ORIGINATOR'S REPORT NUMBER(S)
N00017-70-C-1407	TR-1-71
b. PROJECT NO. NR 215-015	
c.	9b. OTHER REPORT NO(S) (Any other numbers that may be assigned this report)
d.	none

10. DISTRIBUTION STATEMENT

Distribution of this document is unlimited

11. SUPPLEMENTARY NOTES	12. SPONSORING MILITARY ACTIVITY
Contains equations	Office of Naval Research Code 461

13. ABSTRACT

A description is given of the development and corroboration of a simplified computational model for the prediction of the radiated rotational noise of a lifting rotor or propeller. The method is based on a solution of the concentrated force-excited wave equation and the identification of the terms in this solution with annular distributions of monopole sources of specified phase and amplitude.

The computational algorithms developed from this mathematical model provide a rapid means for determining the amplitude and phase of the radiated sound field. They are particularly well suited for providing a description of rotor noise characteristics, which can be used as input to computer programs designed to calculate the rotor noise field in the presence of boundaries.

Results obtained with this method usually differ by less than 4 dB from results obtained by the analytical method of Lowson and Ollerhead. Comparisons of the theory with the experimental cruise data of Schlegal, et al, and with results of whirl-tower tests by Stuckey and Goddard is generally satisfactory. In those cases where the predicted and measured data disagree by more than 5 dB, it is felt that this difference can be explained by the lack of accurate blade-loading data and by experimental error.

DD FORM 1473

Preface

THIS report summarizes the results of a study to develop a mathematical model and computational procedure for characterizing the rotational noise of a helicopter rotor. The resulting data would be suitable as input for computer programs designed to calculate the rotor noise field in the presence of boundaries. This work was performed by the Ordnance Research Laboratory of The Pennsylvania State University under contract NOw 65-0123-d for the Aeronautics Group, Code 461, of the Office of Naval Research, Arlington, Virginia.

Abstract

A DESCRIPTION is given of the development and corroboration of a simplified computational model for the prediction of the radiated rotational noise of a lifting rotor or propeller. The method is based on a solution of the concentrated force-excited wave equation and the identification of the terms in this solution with annular distributions of monopole sources of specified phase and amplitude.

The computational algorithms developed from this mathematical model provide a rapid means for determining the amplitude and phase of the radiated sound field. They are particularly well suited for providing a description of rotor noise characteristics, which can be used as input to computer programs designed to calculate the rotor noise field in the presence of boundaries.

Results obtained with this method usually differ by less than 4 dB from results obtained by the analytical method of Lowson and Ollerhead. Comparisons of the theory with the experimental cruise data of Schlegal, et al, and with results of whirl-tower tests by Stuckey and Goddard is generally satisfactory. In those cases where the predicted and measured data disagree by more than 5 dB, it is felt that this difference can be explained by the lack of accurate blade-loading data and by experimental error.

Table of Contents

Nomenclature

Symbol	Description
$a_m(r,\Theta)$	Coefficient of Fourier series describing blade spatial pressure variations
A	Complex pressure amplitude of monopole source at unit distance
$A_m(r,\Theta)$	Unit-distance amplitude of source monopole at r,Θ for mth sound harmonic
B	Number of blades
c	Chord length
c_0	Speed of sound
$F(r,\Theta,t)$	Complex amplitude of point force expressed in rotor polar coordinates for impulsive chordwise loading
$F'(r,\Theta,t)$	Complex amplitude of force expressed in rotor polar coordinates for rectangular chordwise loading
$F(t-\frac{S}{c_0})$	Retarded force
F_r	Radial force component
h	Rotor (hub) altitude

$h_m(r,\Theta)$	Coefficient of Fourier series for the blade force expressed in rotor polar coordinates
$h_m(x,y,z)$	Coefficient of Fourier series for the blade force expressed in rectangular coordinates
j	$(-1)^{1/2}$
k	Effective ring factor
k_a	$\frac{\omega}{c_0}$
ℓ_1, ℓ_2, ℓ_3	Direction cosines of the force vector coefficient
$L(r,\Theta)$	Blade section loading
m	Sound harmonic number
M	Hub Mach number, $\frac{V}{c_0}$
n(or λ)	Air-load harmonic number
N_s	Number of dipoles in acoustic array model
$p(x,y,z,t)$	Total acoustic pressure at (x,y,z,t)
$p_{m\Theta}(x,y,z)$	Acoustic pressure of mth line component at (x,y,z)
P_r	Dipole pressure at "r" (see Fig. 3)
p_{r0}	Pressure at "r" due to monopole at point "0" (see Fig. 3)
p_{r1}	Pressure at "r" due to monopole at point "1" (see Fig. 3)
$q(t)$	Mass flux rate of monopole
$q'(t)$	Time derivative of mass flux rate of monopole
Q	Rotor torque
r	Rotor polar coordinate (see Fig. 1)

R	Rotor or propeller radius
R_{opt}	Instantaneous distance between moving monopole and receiver
R_{yz}	$[(y_r-y_s)^2+(z_r-z_s)^2]^{1/2}$ (see Fig. 5)
S	$[(x-x_1)^2+(y-y_1)^2+(z-z_1)^2]^{1/2}$ (see Fig. 1)
SPL	Sound pressure level (abbreviation)
t	Time variable
T	Rotor thrust
U_n, V_n	Normalized Fourier coefficients of blade load series
V	Hub velocity
x, y, z	General field point coordinates
x_e	X coordinate of moving monopole at retarded time
x_1, y_1, z_1	General source coordinates
x_i, y_i, z_i	Coordinates of monopole member of ith dipole
X_i, Y_i, Z_i	Coordinates of monopole member of ith dipole corrected for rotor tilt angle
x_{opt}	X coordinate of moving monopole at time "t"
x_r, y_r, z_r	Receiver coordinates
α	Blade angle of attack
β	Angle between source velocity vector and vector joining the source and receiver at retarded time for a moving monopole
γ	An unspecified phase angle
δS	Spacing of monopoles for implementing dipole radiation characteristics

$\Delta\Theta$	Dipole angular separation
Θ	Azimuthal angle (see Fig. 1)
Θ_i	Mean azimuth angle for ith dipole
λ (or n)	Air-load harmonic number
ξ_n	Phase angle for nth air-load harmonic
ξ_c	Blade coning angle
ψ	Rotor tilt angle
ω	Source radian frequency
Ω	Rotor angular velocity (rpm x $2\pi/60$)
Ω_m	$mB\Omega$

An Acoustic-Array Model for the Computation of the Rotational Noise of a Lifting Rotor

THE increasing importance of civilian and military VTOL craft (especially helicopters) has revived interest in the estimation and reduction of propeller- or rotor-generated noise; however, the only rigorous theory that exists applies to the noise from a propeller with symmetrical sections, zero blade angle, and zero forward speed (Ref. 1). There are, however, various approximate analyses that can be used to estimate rotational noise for practical thrust-producing rotors and propellers.

The earliest and still most commonly employed approach to estimating propeller noise is based on a method originally employed by Gutin (see Ref. 2). Basically, this method consists of postulating an approximate pressure distribution over the blades and then using this distribution to calculate the characteristics of independent fixed forces that, when distributed over the area swept by the blades, produce an acoustically equivalent radiation pattern. The radiated sound field is computed as the solution to the appropriate wave equation, assuming the energy source is adequately represented by the fixed-force distribution.

Various extensions and refinements of Gutin's method have been reported in the literature (see, for example, Refs. 3, 4, and 5). These refinements appear to provide the basis whereby reasonably accurate estimates of rotor noise may be obtained, at least for the free-field rotational noise of isolated propellers or helicopter rotors and providing, of course, that proper consideration is given to the effects of nonuniform blade loads.

A more recent method for computing rotor rotational noise stems from the work of Lowson (Ref. 6) who, instead of basing his development on the concept of fixed forces distributed in the blade path, approaches the problem by considering the sound fields arising from singularities in motion. Specifically, equations are derived that describe the general acoustic relationships for a point force in arbitrary motion as well as those for a point source (acoustic monopole) and point acoustic stress in arbitrary motion. Moreover, it is shown how these relationships can be applied to the calculation of various aspects of aircraft noise. These results reduce to those of Gutin for the case of a uniformly loaded propeller.

In practical situations, it is often unsatisfactory to regard propeliers or rotors as isolated noise sources due to the baffling effects of the vehicle fuselage or appendages. Of even greater importance, in some cases, is the necessity of obtaining the noise field of VTOL craft not in the free field but rather in the vicinity of an extended boundary such as the ground or an ocean. In view of these considerations, this study was undertaken to develop a mathematical/computational model of a helicopter rotor (propeller)—a model that:

1. Can be more readily applied to the estimation of rotational noise fields in the presence of boundary surfaces
2. Can provide a simplified method for computing the free-field rotational noise of an isolated rotor for comparison with other data.

Development of the Mathematical Model

The method developed here results in a description of the rotor-system rotational noise in terms of an equivalent array of independent, acoustic-monopole (point), time-harmonic sources. Evidently, this characterization is considered complete once the spatial location, amplitude, and phase of each source in the array are specified.

The principal assumptions made in the course of the mathematical analysis are:

1. Blade angle-of-attack is independent of azimuth
2. The total torque and thrust of the blade system are considered to be concentrated within a thin annular ring located in the path of the blades and at a radius equal to some fraction k of the blade radius
3. The thrust, torque, and radial force vectors operate in phase with one another at any particular point in the blade plane
4. The blade chordwise pressure distribution is assumed to be rectangular and, in the limiting case of an infinitely narrow blade, impulsive
5. Compressibility effects are negligible
6. Transient effects are ignored
7. The acoustic medium is unbounded, homogeneous, and isotropic. The effect of boundaries is handled separately by considering the reflection and transmission of sound at existing boundaries for each simple source in turn and then combining these fields by using the superposition principle.

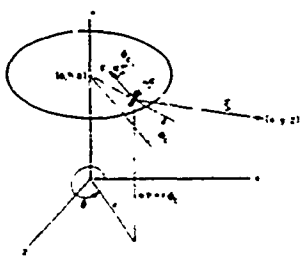

Fig. 1 - Rotor geometry.

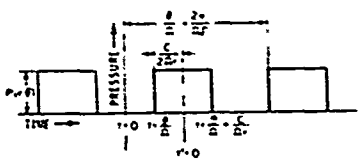

Fig. 2 - Pressure-vs-time history at $(r, \theta, h+r\Omega_c)$.

SPATIAL AND TEMPORAL PRESSURE VARIATIONS IN ROTOR DISK

Figure 1 shows the rotor geometry used in the analysis. The rotor-shaft axis is represented by the y axis; the time and blade azimuthal references are referred to the x axis.

Figure 2 shows an assumed rectangular pressure-versus-time history experienced by a stationary observer located at a

point in the path of the rotor. From this figure it follows that the pressure can be written as a Fourier series:

$$(1) \qquad P(r,\Theta,t) = \sum_{m=1}^{\infty} o_m(r,\Theta) \cos m\Omega B t',$$

where

$$t' = t - \frac{\Theta}{\Omega} - \frac{c}{2\Omega r} ,$$

and

$$o_m(r,\Theta) = \frac{\Omega B}{\Pi} \int_{\frac{-c}{2\Omega r}}^{c/2\Omega r} P(r,\Theta) \cos m\Omega B t' \, dt'$$

or

$$o_m(r,\Theta) = \frac{2P(r,\Theta)}{m\Pi} \sin\frac{mBc}{2r}$$

Note that the m = 0 term has been neglected, since it does not produce an acoustic signal. In terms of blade-section-loading data, i.e.,

$$L(r,\Theta) = c\,P(r,\Theta) ,$$

we have

$$(2) \qquad P(r,\Theta,t) = \sum_{m=1}^{\infty} \frac{2L(r,\Theta)}{m\Pi c} \sin\left(\frac{mBc}{2r}\right) \cos m\Omega B\left(t - \frac{\Theta}{\Omega} - \frac{c}{2\Omega r}\right) .$$

The magnitude of the force corresponding to this pressure is obtained by multiplying Eq. 2 by r·dr·dΘ:

$$(3) \qquad F'(r,\Theta,t) = \sum_{m=1}^{\infty} \frac{2rL(r,\Theta)}{m\Pi c} \sin\left(\frac{mBc}{2r}\right) \cos m\Omega B\left(t - \frac{\Theta}{\Omega} - \frac{c}{2\Omega r}\right) dr d\Theta .$$

The rectangular pressure distribution assumed in the derivation of the preceding equation leads to results that tend to deemphasize or even eliminate certain rotor-noise line components due to the presence of the factor (1/m)sin(mBc/2r). This behavior is not generally observed in experimental data; however, precise definition of the chordwise pressure distributions can be expected to be significant only at frequencies at which the wavelength is not greater than the order of a chord length (see Ref. 7). Accordingly, for most practical cases that arise in rotor-noise calculations, one finds that a point-loading distribution (impulse) is adequate for the purpose of representing the actual distributed chordwise pressure distribution. In addition to its mathematical simplicity, the impulsive loading assumption has the advantage that it leads to results that appear to be more nearly reflected by available experimental data. Other chordwise pressure distributions can be accounted for by reevaluating Eq. 1.

An expression equivalent to Eq. 3 for point (impulsive) loading can be easily derived in the limiting case of small chord length. In fact, since

$$\lim_{c\to 0} \frac{\sin(m\mathcal{B}c/2r)}{(m\mathcal{B}c/2r)} = 1 \quad ,$$

it follows from Eq. 3 that the expression describing the amplitude and phase of the point force at (r, Θ, t) is

$$F(r,\Theta,t) = \sum_{m=1}^{\infty} \frac{B}{\Pi} L(r,\Theta) \cos m\Omega B\left(t - \frac{\Theta}{\Omega}\right) dr d\Theta \quad . \tag{4}$$

ACOUSTIC RELATIONS

We begin with the force-driven wave equation, which relates the acoustic pressure to the driving-force vector:

$$\nabla^2 p - \frac{1}{c_0^2} \frac{\partial^2 p}{\partial t^2} = \vec{\nabla} \cdot \vec{F} \quad . \tag{5}$$

In the limit of a point-applied force, the solution to Eq. 5 is (see Ref. 8)

$$p = -\frac{1}{4\Pi} \vec{\nabla} \cdot \left[\frac{\vec{F}(t - S/c_0)}{S}\right] \quad , \tag{6}$$

where

$$S^2 = (x - x_1)^2 + (y - y_1)^2 + (z - z_1)^2 \quad .$$

When the force vector at a point in the rotor disk can be represented as a Fourier series, such as

$$\vec{F}(r, \Theta, t) = \sum_{m=1}^{\infty} \vec{h}_m(r,\Theta) \cos(\Omega_m t + \gamma) \quad , \tag{7}$$

then the solution (Eq. 6) may be written as

$$p(x,y,z,t) = -\frac{1}{4\Pi} \sum_{m=1}^{\infty} \vec{h}_m(x,y,z) \cdot \vec{\nabla} \left\{\frac{\cos[\Omega_m(t - S/c_0) + \gamma]}{S}\right\} . \tag{8}$$

Now, since we can write the force-vector coefficient in terms of its magnitude $h_m(x,y,z)$ and its direction cosines ℓ_1, ℓ_2, and ℓ_3, Eq. 8 becomes

$$p(x,y,z,t) = -\frac{1}{4\Pi} \sum_{m=1}^{\infty} \left[h_m(x,y,z)\right] \left[\ell_1 \frac{\partial}{\partial x} + \ell_2 \frac{\partial}{\partial y} + \ell_3 \frac{\partial}{\partial z}\right] \left\{\frac{\cos\left[\Omega_m\left(t - \frac{S}{c_0}\right) + \gamma\right]}{S}\right\} \quad . \tag{9}$$

But

$$\ell_1 \frac{\partial}{\partial x}\left\{\frac{\cos\left[\Omega_m\left(t-\frac{S}{c_0}\right)+\gamma\right]}{S}\right\}=\ell_1\left\{\cos\left[\Omega_m\left(t-\frac{S}{c_0}\right)+\gamma\right]\right.$$

$$\left.-\frac{S\Omega_m}{c_0}\sin\left[\Omega_m\left(t-\frac{S}{c_0}\right)+\gamma\right]\right\}$$

$$\frac{\partial}{\partial x}\left(\frac{1}{S}\right) ,$$

with similar relations for the partial derivatives with respect to y and z. In the above we have used the fact that

$$\frac{\partial}{\partial x}\left(\frac{1}{S}\right)=-\frac{1}{S^2}\frac{\partial}{\partial x}(S)$$

(and similarly for the y and z derivatives) so that we can rewrite Eq. 9 as

$$p(r,y,z,t)=-\frac{1}{4\Pi}\sum_{m=1}^{\infty}\left[h_m(x,y,z)\right]\left\{\cos\left[\Omega_m\left(t-\frac{S}{c_0}\right)+\gamma\right]-\frac{S\Omega_m}{c_0}\right.$$

$$\left.\sin\left[\Omega_m\left(t-\frac{S}{c_0}\right)+\gamma\right]\right\}\left[\ell_1\frac{\partial}{\partial x}+\ell_2\frac{\partial}{\partial y}+\ell_3\frac{\partial}{\partial z}\right]\left(\frac{1}{S}\right) ,$$

or

$$p(x,y,z,t)=\frac{1}{4\Pi}\sum_{m=1}^{\infty}\left[h_m(x,y,z)\right]\left[1+\left(\frac{S\Omega_m}{c_0}\right)^2\right]^{1/2} \tag{10}$$

$$\cos\left[\Omega\left(t-\frac{S}{c_0}\right)+\gamma+\phi\right]\frac{\cos\psi}{S^2} ,$$

where

$$\phi=\tan^{-1}\left(\frac{S\Omega_m}{c_0}\right) ,$$

and

$$\cos\psi=\frac{\vec{h}_m\cdot\vec{S}}{h_m S}$$

Equation 10 is in a form that can be recognized as the pressure field arising from the summation of an infinite series of dipole acoustic sources. For example, consider a pair of acoustic monopoles of frequency ω located at P_0 and P_1 as in Fig. 3. Here it is assumed that the pressure field at P_r due to the monopole at P_1 is given by

$$p_{r1}=\frac{A_1}{S'}\cos\left[\omega\left(t-\frac{S'}{c_0}\right)+\gamma\right] ,$$

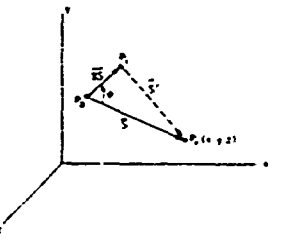

Fig. 3 - Dipole source geometry.

and that for the monopole at P_0 is

$$p_{r0} = -\frac{A_1}{S} \cos\left[\omega\left(t - \frac{S}{c_0}\right) + \gamma\right]$$

In the limit as δS becomes small it can be shown (Ref. 9) that the pressure field at P_r due to the dipole source composed of the two given monopoles can be expressed as

$$(11) \qquad p_r = |\delta S| A_1 \left[1 + \left(\frac{\omega S}{c_0}\right)^2\right]^{1/2} \cos\left[\omega\left(t - \frac{S}{c_0}\right) + \gamma + \phi\right] \frac{\cos\psi}{S^2} \quad ,$$

where

$$\cos\psi = \frac{\vec{\delta S} \cdot \vec{S}}{\delta S \; S} \quad ,$$

$$\phi = \tan^{-1}\left(\frac{S\omega}{c_0}\right) \quad ,$$

and γ is an arbitrary initial phase angle. From a comparison of Eqs. 10 and 11 it is evident that the pressure field in Eq. 10 is made up of monopole sources for which

$$(12) \qquad A_m(r,\Theta) = \frac{h_m(r,\Theta)}{4\Pi\delta S} \quad .$$

We can now relate Eq. 12 to Eq. 4, which was derived to describe the amplitude of the force whose line of action is along the vector $\vec{\delta S}$. For a force directed to produce a net lift on a horizontal rotor system, as in Fig. 1, we find that

$$(13) \qquad h_m(r,\Theta) = \frac{B}{\Pi} L(r,\Theta)\, dr d\Theta \quad ,$$

and the line of action of the force vector, as well as $\vec{\delta S}$, can be taken to be normal to the blade chord. If we now make use of the assumption that the rotor forces are concentrated within an "effective ring" located at a radius equal to $k\Omega$, we can avoid the radial integration implied by Eq. 13 and, using a harmonic series for the normalized blade-loading data, write

$$(14) \qquad L(r,\Theta)\, dr \approx \left[T^2 + \left(\frac{Q}{k\Omega}\right)^2 + F_r^2\right]^{1/2} \left(\frac{1}{B}\right)\left\{1 + \sum_{n=1}^{\infty}\left[U_n^2 + V_n^2\right]^{1/2} \cos\left[n(\Theta - \Theta_r) - \xi_n\right]\right\}$$

It is noteworthy that the effective-ring approximation has long been used in the application of propeller-noise theory, and it has the effect of simplifying the computations—usually without introducing severe errors. With regard to its use in predicting helicopter noise, Lowson and Ollerhead (Ref. 7) point out that, under the assumption of random loading-phase variations around the rotor azimuth and along the blade span, the error arising from

consideration of only one radial station (i.e., a single effective ring) is small, at least in the far field. A representative figure for the location of a single effective ring is taken to be the 80 percent radial station (k=0.8).

The amplitude of the monopole sources comprising the equivalent rotor noise model of the mth line component of rotational noise can be computed by combining Eqs. 12, 13, and 14:

$$(15) \qquad |A_m(kR,\Theta)| = \frac{F_t}{4\Pi^2 \delta S}\left\{1+\sum_{n=1}^{\infty}\left[U_n^2+V_n^2\right]^{1/2}\right.$$

$$\left.\cos\left[n(\Theta-\Theta_r)-\xi_n\right]\right\}\Delta\Theta \quad ,$$

where

$$F_t = \left[T^2+\left(\frac{Q}{kR}\right)^2+F_r^2\right]^{1/2} \quad ,$$

and where the symbol for the infinitesimal $d\Theta$ has been replaced by the source angular separation $\Delta\Theta$. Thus, it is proposed to model the acoustic field of the lifting rotor by means of two circular arrays of phase- and amplitude-shaded monopoles arranged as shown in Fig. 4. Here, the upper ring of sources is composed of positive monopoles whose amplitude and phase are related to the azimuthal angle assigned to each monopole by the expression

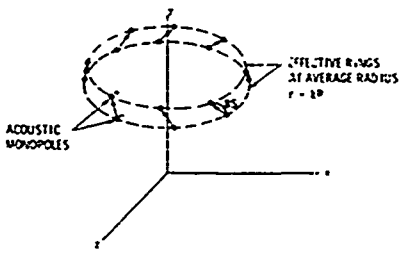

Fig. 4 - Example of rotor acoustic-array model.

$$(16) \qquad A_m(kR,\Theta) = \frac{F_t}{4\Pi^2 \delta S}\left\{1+\sum_{n=1}^{\infty}\left[U_n^2+V_n^2\right]^{1/2}\cos\left[n(\Theta-\Theta_r)-\xi_n\right]\right\}$$

$$\cos m\Omega B\left(t-\frac{\Theta}{\Omega}\right)\Delta\Theta \quad .$$

The lower monopole ring is composed of sources of opposite sign. Note that the two source rings are slightly displaced from one another in azimuth (and have slightly different diameters) so that the dipole vectors are aligned with the blade force vectors.

The acoustic field of the mth line component developed at a field point with coordinates x, y, z due to the operation of the monopole at x_1, y_1, z_1 (kR, Θ in rotor polar coordinates) follows immediately from Eq. 16:

$$(17) \qquad p_{m\Theta}(x,y,z) = \pm\frac{F_t}{4\Pi^2 S\delta S}\left\{1+\sum_{n=1}^{\infty}\left(U_n^2+V_n^2\right)^{1/2}\cos\left[n(\Theta-\Theta_r)-\xi_n\right]\right\}$$

$$\cos m\Omega B\left(t-\frac{S}{c_0}-\frac{\Theta}{\Omega}\right)\Delta\Theta \quad .$$

In Eq. 17 the plus sign is used for monopoles in the upper ring and the minus sign for those in the lower ring. The total acoustic

pressure due to all the sources in the array is obtained simply by superimposing the effects of the individual sources at the receiver. This computation is readily adapted for machine implementation.

SPATIAL RELATIONS

The basic rotational noise model has been described in terms of an array of phase- and amplitude-shaded acoustic monopoles, it remains to establish the number and spatial location of the sources in the array.

It is convenient to specify the location of the source rings so that the mean rotor height (h) is midway between the two y coordinates describing the upper and lower ring heights. If the azimuthal angle Θ is referred to the horizontal plane located at the mean rotor height (and with $\Theta=0$ in the direction of the positive x axis), the location of the monopoles may be specified using the blade angle of attack α, the coning angle ϕ_c, and the mean azimuth angle Θ_i corresponding to the ith dipole. In fact, the coordinates of the two monopoles comprising the ith dipole are:

$$x_i^{\pm} = r\cos\Theta_i \pm \frac{\delta S}{2}\left[\sin\alpha\sin\Theta_i - \cos\alpha\cos\Theta_i\sin\phi_c\right] \tag{18}$$

$$y_i^{\pm} = h \pm \frac{\delta S}{2}\cos\alpha\cos\phi_c$$

$$z_i^{\pm} = -r\sin\Theta_i \pm \frac{\delta S}{2}\left[\sin\alpha\cos\Theta_i + \cos\alpha\sin\Theta_i\sin\phi_c\right]$$

where the upper sign is used for the sources in the upper ring and the lower sign for the sources in the lower ring.

The case of a rotor (or propeller) arbitrarily oriented with respect to the assumed coordinate system is handled by straightforward coordinate transformation once the equivalent acoustic array is computed for the horizontal rotor configuration. The transformation employed here uses a rotor tilt angle ψ which specifies the inclination of the rotor disk relative to the x-z plane. The positive x axis is used as the angle reference and an upward tilt of the rotor plane is defined as positive. Parenthetically, it should be mentioned that it is considered unnecessary to provide for rotation of the blade system about the rotor axis, since the same relative effect can be obtained by selecting appropriate field point (receiver) coordinates. Thus, the transformation equations may be written as:

$$X_i^{\pm} = \left(x_i^{\pm}\right)\cos\psi - \left[\left(y_i^{\pm}\right) - h\right]\sin\psi \tag{19}$$

$$Y_i^{\pm} = h + \left(x_i^{\pm}\right)\sin\psi + \left[\left(y_i^{\pm}\right) - h\right]\cos\psi$$

$$Z_i^{\pm} = z_i^{\pm}$$

To retain adequate fidelity in the process of computationally simulating the rotor noise sources, it is necessary to provide a sufficient number of dipoles in the approximation to the rotor noise continuum. The basic consideration is one of using enough dipoles, equally spaced around the effective ring, to satisfy Shannon's sampling theorem for the highest air-load harmonic to be considered.

The problem of estimating the range of air-load harmonics required for the computation of the rotational noise of the mth line component was considered by Lowson and Ollerhead (Ref. 7). They concluded that, for accuracy, air-load data must be included in the range given by the expression

$$mB(M-1) \leq \lambda \leq mB(M+1) \quad . \tag{20}$$

Accordingly, to provide an adequate number of dipoles in the simulation of the highest air load, it is necessary that

$$N_s \geq 2mB(M+1) \quad . \tag{21}$$

For the third acoustic line component of the SH-3A (HSS-2) helicopter rotor, for example, Eq. 21 specifies that about 44 dipoles (88 monopoles) should be used for the highest required air-load harmonic (the 22nd).

Another quantity that must be provided when using the model is the magnitude of the monopole spacing δS. Generally, it has been found that the relation

$$\delta S = 0.01 \frac{2\pi c_0}{mB\Omega} \tag{22}$$

gives good results computationally.

The Computational Model

The computational model consists of algorithms for specifying the location (x_1, y_1, z_1 coordinates), amplitude (at unit distance), and relative phase of each source in an acoustic array designed to simulate the rotor noise. Equations 16 and 19 are the basic expressions that describe these quantities.

From Eq. 16, which gives the strength and phase of a monopole in the circular array, we note that rather detailed knowledge of the blade loading distribution is assumed. Unfortunately, blade loading characteristics are not well known at present. For example, no information is available that will permit one to calculate the phase angle ξ_n. Furthermore, information on the blade-load amplitudes (U_n and V_n) is empirical and is based chiefly on the in-flight measurements reported by Scheiman (Ref. 10), which were conducted using an instrumented helicopter.

Using Scheiman's data, together with that of Burpo and Lynn (Ref. 11), Lowson and Ollerhead (Ref. 7) proposed a loading law for the blade-load amplitudes based on the inverse 2.5 power of the blade-loading harmonic number λ assuming use of the effective-

ring approximation. To circumvent the specification of individual phase angles ξ_n, they further assumed that the acoustic contributions of the various air-load harmonics could be combined in the mean-squared sense.

The proposed acoustic-array geometry that emerges as a result of the above considerations is composed of a number of circular arrays similar to that shown in Fig. 4. Due to the fact that the ξ_n are as yet unknown, however, a single equivalent array for the rotor noise field cannot be obtained. Instead, it is necessary to employ individual circular arrays to account for the contributions from each of the air-load harmonics considered and to sum the resultant acoustic fields in the mean-squared sense as suggested above.

CORRECTIONS FOR ROTOR-SYSTEM TRANSLATION

It is convenient to account for the effects of rotor-system translation by applying the proper uniform-motion corrections to the pressure field of each monopole before superimposing their individual contributions at the receiver. For the case of a stationary observer located at coordinates (x_r, y_r, z_r), and for uniform subsonic hub motion in the direction of the positive x axis, the appropriate corrections can be derived beginning with the results of Morse and Ingard (Ref. 12). After a few typographical errors in Eq. 11.2.15 of the above reference are corrected, one can write this equation as

$$(23) \qquad p = \frac{1}{4\pi} \frac{q'\left[t-\frac{R_r}{c_o}\right]}{R_r(1-M\cos\beta)^2} + \frac{q\left[t-\frac{R_r}{c_o}\right](\cos\beta - M)V}{4\pi R_r^2(1-M\cos\beta)^3} \quad .$$

This equation expresses the observed pressure from a moving monopole in terms of the rate of mass flux out of the source (i.e., its strength $q(t)$, the time derivative of the mass flux rate $(q'(t))$, the source-to-receiver distance at retarded time (R_r), and the angle between the source velocity vector and the vector joining the source and receiver at retarded time (β).

For a harmonic monopole source whose pressure field at unit distance is given by the expression

$$p = A\, e^{j\omega t} \quad ,$$

Eq. 23 takes the form

$$(24) \qquad p = \frac{A\, e^{j(\omega t - k_o R_r)}}{R_r(1-M\cos\beta)^2} \left[1 - j\,\frac{(\cos\beta - M)M}{k_o R_r(1-M\cos\beta)}\right] \quad .$$

To compute the appropriate values of R_r and β, we make use of the geometry shown in Fig. 5. We note that, without loss of generality, the motion of the source may be taken to be along a line parallel to the x axis and at a distance z_s from the y axis. The instantaneous position of the source is given by the coordinates (x_s, y_s, z_s); the source position when the sound was emitted

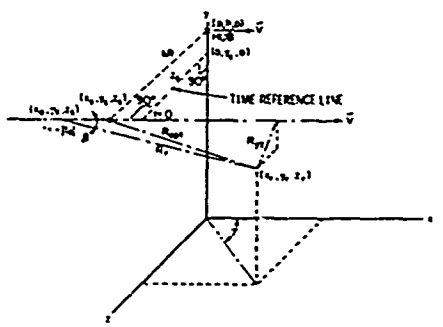

Fig. 5 - Source-motion geometry.

is (x_e, y_S, z_S). Therefore, the "optical," or instantaneous, distance between the source and receiver is R_{opt}; whereas, the distance between the source and receiver at the instant the sound was emitted is R_r. From Fig. 5 it is not difficult to show that

$$R_r = \frac{-M\, x_{opt} + \left[(x_{opt})^2 + (1-M^2) R_{yz}^2 \right]^{1/2}}{1-M^2} , \tag{25}$$

and

$$\cos\beta = \frac{(x_r - x_e)}{|x_r - x_e|} \left[1 - \left(\frac{R_{yz}}{R_r} \right)^2 \right]^{1/2} , \tag{26}$$

where

$$x_{opt} = x_s - x_r$$

and

$$R_{yz} = \left[(y_r - y_s)^2 + (z_r - z_s)^2 \right]^{1/2} .$$

Thus, given the location (x_S, y_S, z_S), as well as the amplitude and phase (A) of the source, Eq. 24 can be used to compute the contribution of the source at the stationary receiver position for any subsonic value of the hub convection Mach number, $M = V/c_0$.

Illustrative Examples

The first test of the mathematical model was made by comparing various computational results with those obtained using the method suggested by Lowson and Ollerhead (Ref. 7). To maintain reasonably close correspondence between the two techniques, the present computations were also carried out using the assumptions embodied in:

1. A loading law for the harmonic amplitudes
2. A 10:1:1 relationship between the magnitudes of the force vectors for T, Q, and F_r
3. A random phase relationship between the acoustic contributions of the various air loads
4. The effective-ring approximation.

Note that these assumptions are not indigenous to the present computational procedure. In fact, the first two assumptions can be eliminated by the simple expedient of providing the computer program with data cards that describe some other set of loading amplitudes, phases, and force-component magnitudes; whereas the remaining two can be eliminated by making only minor changes in the computational algorithms.

Figure 6 is a polar plot of the predicted sound patterns for the first three line components of a Sikorsky S-58 helicopter rotor in the hover configuration. These sound patterns were

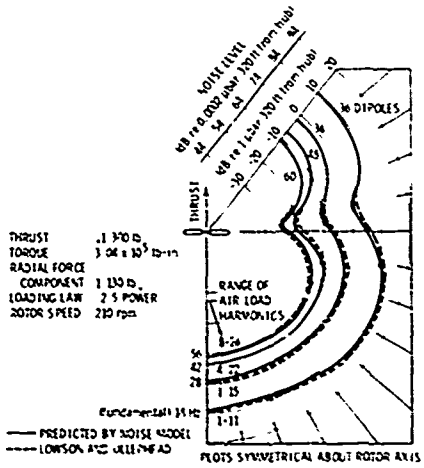

Fig. 6 - Free-field sound patterns of the Sikorsky S-58 (HSS-1) helicopter in hover configuration.

computed for a radial distance from the hub of 320 ft; therefore, they are approximately representative of free-field conditions. The figure also includes the number of azimuthal stations (number of dipoles) as well as the range of air-load harmonics (λ) used by the digital program. The very close agreement between the results of the two techniques is evident.

Figure 7 shows the predicted sound patterns for four line components of the SH-3A rotor in the hover configuration. Again the data are in close correspondence. The predicted sound patterns for four line components of the same rotor at a radial distance much nearer to the hub and essentially in the near field of the rotor is shown in Fig. 8. At this distance the far-field assumptions inherent in the method of Lowson and Ollerhead are probably unjustified; nevertheless, it can be seen that the data produced by use of the two methods are in close agreement.

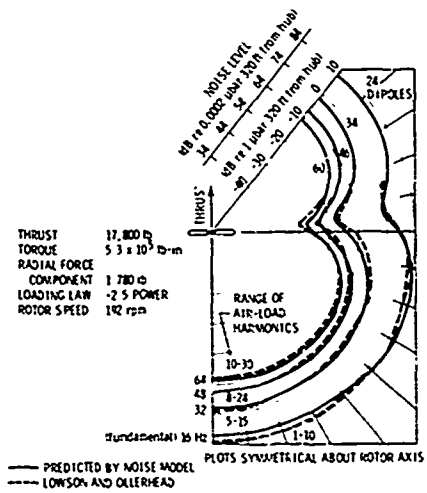

Fig. 7 - Free-field sound patterns of the Sikorsky SH-3A (HSS-2) helicopter in hover configuration.

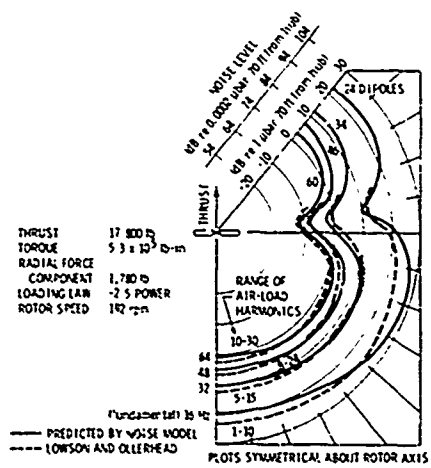

Fig. 8 - Near-field sound patterns of the Sikorsky SH-3A (HSS-2) helicopter in hover configuration.

In general, use of the present computational procedure to accurately predict the near-field noise of a helicopter rotor requires that reliable data on the loading phase variations be used and that the assumption of an effective ring be discarded. Nevertheless, it appears that useful data can be obtained in many cases even if these refinements are not made. In particular, this conclusion seems to be valid for field points outside the sphere defined by the path of the rotor tip.

Figures 9, 10, and 11 illustrate the calculated effects of forward speed on the sound patterns; they show the instantaneous sound patterns for the SH-3A rotor at steady forward flight speeds of 120, 80, and 40 knots. For comparison, several representative data points calculated by the method of Lowson and Ollerhead are provided for the 120-knot case (Fig. 9). Again the two methods yield similar results.

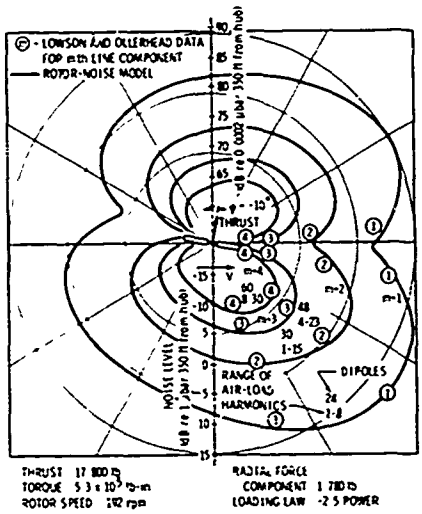

Fig. 9 - Effect of forward speed on the sound patterns of the SH-3A helicopter rotor in steady flight at a forward speed of 120 knots.

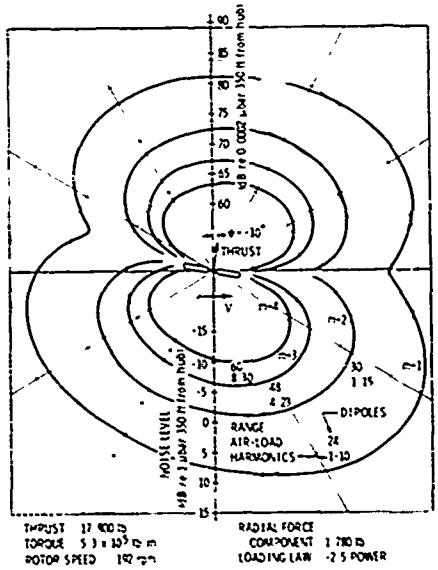

Fig. 10 - Effect of forward speed on the sound patterns of the SH-3A helicopter rotor in steady flight at a forward speed of 80 knots.

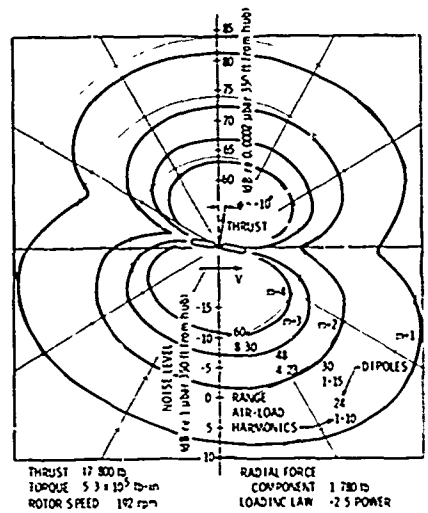

Fig. 11 - Effect of forward speed on the sound patterns of the SH-3A helicopter rotor in steady flight at a forward speed of 40 knots.

To test the present theory against measured data, sound pressure levels corresponding to the "flyby" (cruise) measurements reported by Schlegal, et al, were calculated for the S-58 helicopter. These data correspond to the 40-, 80-, and 110-knot cruise cases and for the first four acoustic line components at each speed. For all cases the helicopter altitude was 200 ft and the sound level was measured by a stationary observer located near the ground and at a point 250 ft off the flight path.

The flyby data referred to above are compared in Figs. 12, 13, and 14. These figures contain data from Ref. 4 on the measured SPL for two runs at each cruise speed together with a

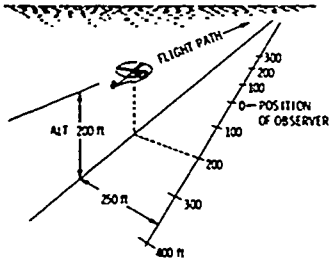

Run geometry for Figs. 12, 13, and 14

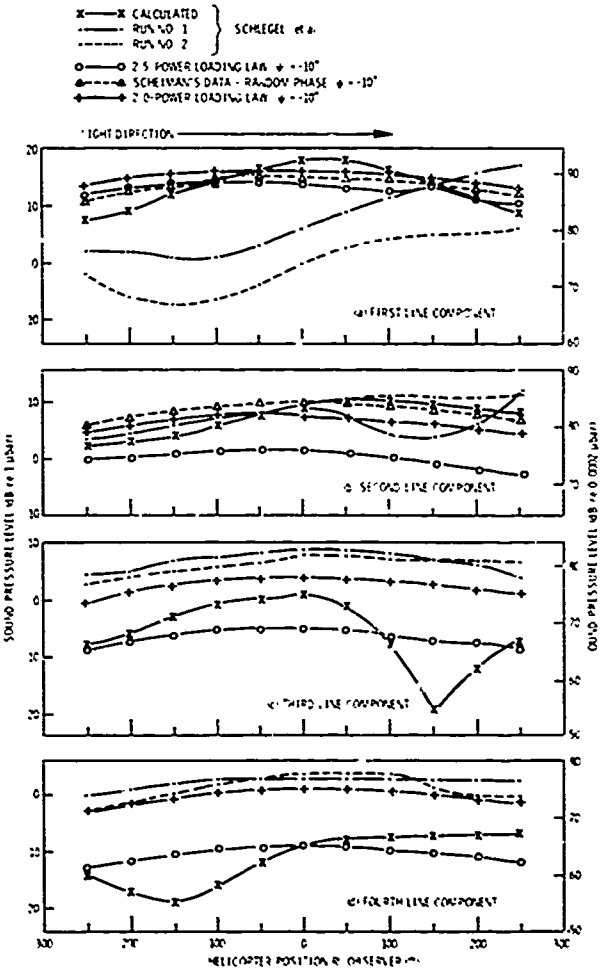

Fig. 12 - Sound pressure levels (flyby data) for the S-58 helicopter at a cruising speed of 40 knots.

curve calculated by the theory presented therein. In addition to these data, three curves computed by the present theory are included on the figures corresponding to the first two line components of each speed run. Two of these curves represent calculated data based on 2.0 and 2.5 inverse power laws for the harmonic amplitudes and the assumption of random phase relationships between the sound contributions of the loading harmonics. The third curve computed by the present method uses the air-load amplitude data reported by Scheiman for the appropriate cruise case, although the phases of the sound contributions of each air-load harmonic are again assumed to be random. The helicopter data used as input for these calculations are given in Table VI of Ref. 4.

For the third and fourth line components of each speed run only two comparative curves are provided in the figures for the present computational method. The curve computed from the Scheiman data is omitted because the number of loading harmonics is insufficient to permit calculation of acoustic line components above the second for the S-58 rotor system. Thus, it is to be

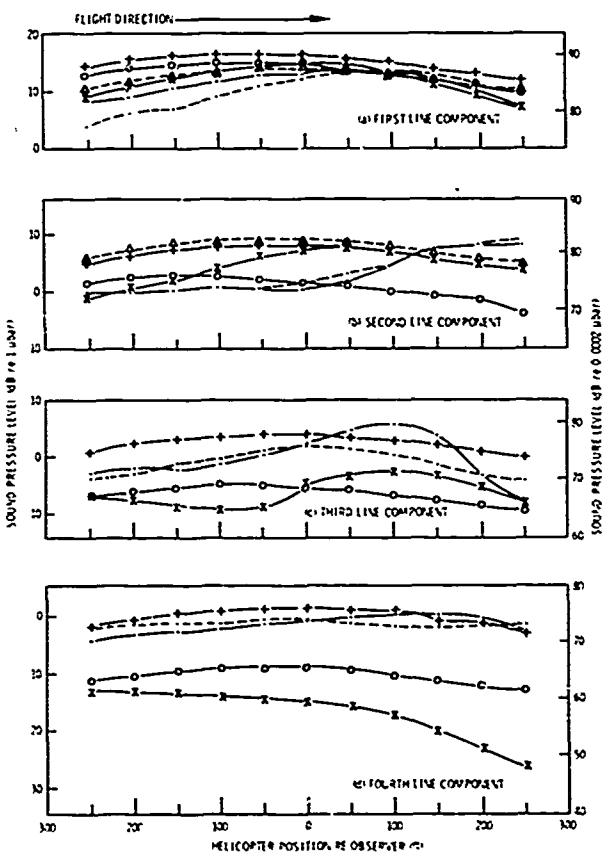

Fig. 13 - Sound pressure levels (flyby data) for the S-58 helicopter at a cruising speed of 80 knots.

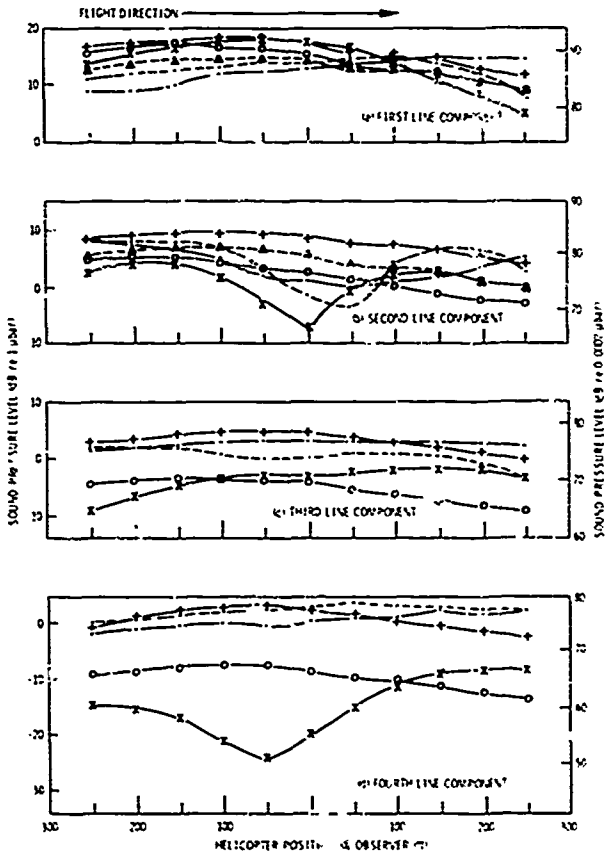

Fig. 14 - Sound pressure levels (flyby data) for the S-58 helicopter at a cruising speed of 110 knots.

expected that the theoretical curve derived in Ref. 4 (using Scheiman's data) would demonstrate progressively poorer correspondence with measured data as higher-frequency line components are considered. This observation is borne out by the cruise-data comparisons. For example, it can be seen that the 2.0 power loading-law assumption leads to significantly better results for the third and fourth acoustic line component data (Figs. 12c, 12d, 13c, 13d, 14c, and 14d). The loading-law computations include the effects of harmonic loading contributions up to the 18th for the third line component and up to the 24th for the fourth line component. It is conceivable that the use of this many measured loading-amplitude terms in the calculations would lead to more consistently accurate results than the use of a loading "law." Nevertheless, it will probably be some time before the blade-loading characteristics can be measured or otherwise specified in sufficient detail to render the use of a loading law unnecessary, particularly for the calculation of the higher line components of the rotor.

As a final comparison of theory with experiment, calculations were made to compare the present rotor-noise model with a set of results from whirl-tower tests reported by Stuckey and Goddard (Ref. 13). The result of this comparison is shown in Fig. 15. Note that calculations were made for the case of steady loading as well as for the cases corresponding to 2.5- and 2.0-power loading laws. Once again, the result with the 2.0-power loading law is seen to be superior to that with the 2.5-power law.

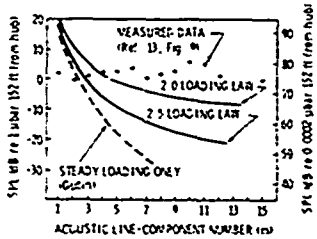

Fig. 15 - Comparison of theory with results of whirl-tower tests for a three-bladed rotor.

The largest discrepancies between theory and experiment in Fig. 15 occur for the first two acoustic line components. However, the accuracy of the measured data at these frequencies is open to question and, in fact, Stuckey and Goddard point out that data for the first, second, and third line components are suppressed due to the limited frequency response of the amplifier and microphone. In addition, the authors also point out that the higher harmonics are exaggerated due to reflections from surrounding structures and to reingestion effects. Thus, it appears that agreement between theory and experiment for the case shown in Fig. 15 may actually be better than the available data indicate.

Note that in the above it has been assumed that the effective ring factor is 0.8 for every air-load harmonic considered. To be more precise, it should be recognized that the value of this air-load factor is a function of the particular air load under consideration. However, since the effect of this refinement on the radiated noise is usually small and data on its specification is normally unavailable, it is frequently more expedient to ignore it.

Appendix

Fortran Listing of Computer Program Implementation of the Acoustic-Source Model

THE digital-computer program presented in this appendix was written to provide a rapid means of evaluating Eqs. 16 and 19 and to produce punched-card and printed output specifying the location, strength, and phase of the monopoles comprising the acoustic array model of rotor rotational noise. In addition, the program provides for the computation of the polar patterns (in a vertical plane) corresponding to the acoustic fields of each air-load harmonic contribution as well as the total estimated sound field obtained by mean-squared addition of these individual contributions.

Specification of the air-load harmonics is accomplished either by providing a nonzero value for the loading-law exponent (LOADL W) or by means of punched-card input that provide values for the harmonic number and normalized amplitude and phase for each air-load harmonic used. In the latter case the parameter LOADLW is set equal to zero. The highest air-load harmonic to be considered is specified by the parameter NHARM, and the lowest (starting) harmonic to be considered by the parameter NSTART. For example: NSTART=1 specifies consideration of all air-load harmonics beginning with the fundamental (steady-only component) and concluding with the harmonic number corresponding to the value of NHARM.

Although the digital program presented here is arranged to provide polar pattern data for the resulting sound fields, it is a simple matter to modify it to handle arbitrarily specified receiver points. In fact, such a modification was used in the calculation of the flyby cruise data. In this case data cards giving the cartesian coordinates of the receiver points (XR, YR, and ZR) were used instead of the algorithm contained between statement number 19 and number 21.

If it is desired to account for the phases of the harmonic loading terms, it is necessary to sum their contributions to the

sound field directly rather than in the mean-squared sense. The printed output provides the magnitude and phase of each air-load contribution so that this computation may be carried out.

At the conclusion of the program, control will return to the first READ statement, and a new set of input data cards will be processed. Thus, to terminate the program execution, a blank card should be inserted after the last set of data cards.

```
C      THIS PROGRAM COMPUTES THE LOCATION STRENGTH AND PHASE OF THE
C      ACOUSTIC POINT SOURCE APPROXIMATION TO THE FORCE DIPOLE FIELD
C      USING THE EFFECTIVE RING PROPELLER MODEL
C      J.MACALUSO ORL  VERSION 5 9/17/70 MOD 03
C
C      PRINCIPAL PROGRAM SYMBOLS AND UNITS ARE -
C
C      QUANTITY                        SYMBOL          UNITS/REMARKS
C
C      MAGNITUDE OF BLADE-
C      LOADING HARMONIC                AHARM(I)        NORMALIZED BY STDY TRM
C      BLADE ANGLE AT K*R              ALPHA           RADIANS
C      PHASE ANGLE OF BLADE-
C      LOADING HARMONIC                APHSE(I)        INPUT IN DEG
C      FLD PT VERT ANGLE               BETA            RADIANS
C      CHORD AT KR                     C               FT
C      VELOCITY OF SOUND               CO              FT/SEC
C      CONVERSION FACTOR               CVFCTR          PSI TO MICROBARS
C      ANGULAR SPACING OF
C      FIELD POINTS                    DBETA           INPUT IN DEG
C      MONOPOLE SPACING                DELS            FT
C      FREQ OF M'TH HARM
C      LINE COMPONENT                  FNDFRQ          HZ(NO DOPPLER)
C      RADIAL FORCE COMPONENT          FRAD            LBS
C      MAG OF TOTAL BLADE FORCE
C      AT K*R                          FRCMAG          LBS
C      DISK ROTATION RATE              FRFQ0           HZ
C      FLD POINT HORIZ ANGLE           GAMMA           INPUT IN DEG
C      ROTOR HEIGHT                    H               FT
C      EFFECTIVE RING FACTOR           K               FXD PT IN TENTHS
C      MAG OF LOAD LAW EXP             LOADLW          USED WHEN AIRLD DATA
C                                                      SUPPLIED ONLY BY LOADLW
C                                                      OTHERWISE SET EQ ZERO
C      ORDER OF HARMONIC               M               ------
C      HUB CONVECTION MACH NMBR        MACH            MOTION RE +X AXIS
C      NUMBER OF BLADES                NB              ------
C      NO OF FIELD POINTS              NFP             ------
C      NUMBER OF BLADE
C      AIRLOAD HARMONICS               NHARM           ------
C      FLAG-POLAR PLOT DATA            NPLOT           IF=1 DATA OUTPUTTED
C      FLAG-SOURCE(I,J) PNCHED         NPNCH           IF=1 DATA OUTPUTTED
C      FLAG-SOURCE(I,J) PRINT          NPRNT           IF=1 DATA OUTPUTTED
C      NO.SOURCE DIPOLES               NSOPLS          ------
C      LOWEST LOADING HARM.            NSTART          ------
C      SHAFT ANG VELOCITY              OMEGA           RAD/SEC
C      RADIAL FORCE ANGLE              PHIC            ATAN(FRAD/T)
C      ROTOR TILT ANGLE                PSI             DEG(POS. UP RE HORIZ.)
C      TOTAL TORQUE                    Q               INPUT IN LB-INCHES
C      (AZIMUTH FUNDAMENTAL)
C      BLADE RADIUS                    R               FT
C      FIELD POINT RADIUS              RFP             FT
C      RPM                             RPM             REV/MIN
C      MONOPOLE SOURCE MATRIX          SOURCE(I,J)     MIXED UNITS
C      TOTAL THRUST                    T               LBS
C      (AZIMUTH FUNDAMENTAL)
C      ROTOR AZIMUTH ANGLE             THETA           RADIANS
C      BLADE LOAD REF ANGLE            THETAR          INPUT IN DEG
C      HUB VELOCITY(CONST)             V               KNOTS INPUT(SUBSONIC)
C      RECEIVER COORDINATES            XR,YR,ZR        FT
C
```

```
C     ******************************************************************
C
      DIMENSION  SOURCE(5,2000),AHARM(50),APHSE(50),ANSTOT(2,100)
      REAL*8 SOURCE,DIST,DBLP,ARG,AIMAG,REAL,LOADLW*4,MACH*4,TWOPI
      NAMELIST/DATIN/M,NFP,RFP,DBETA,H,T,Q,RPM,NB,K,CO,C,R,LOADLW,FRAD,
     1V,GAMMA/DATUSE/NSOPLS,PHIC,MACH
     2,Q,FQ,ALPHA,DELS,DTHETA,OMEGA,FREQO,FNDFRQ,NHARM,NSTART,THETAR,PSI
C     READ INPUT DATA
    1 READ(5,2)NB,K,CO,C,R,PSI,THETAR,LOADLW,V,NPLOT,NPRNT,NPNCH,NHARM,
     1NSTART,NSOPLS
      IF(NB.EQ.0) GO TO 24
    3 READ(5,4) M,NFP,RFP,DBETA,GAMMA,H,T,Q,FRAD,RPM
    2 FORMAT(2I5,E10.3,6F5.2,6I5)
    4 FORMAT(2I5,4F5.1,4E10.3)
C     PRINT CAPTION AND INPUT DATA FOR THIS RUN
      WRITE(6,5)
      WRITE(6,DATIN)
    5 FORMAT(1HO,'COMPUTATION OF EFFECTIVE RING DATA-VERSION 5 9/17/70
     1MOD03'/1HO,'INPUT DATA FOLLOWS-'//)
C     COMPUTE AND IDENTIFY RUN CONSTANTS
      PI=3.1415926
    6 TWOPI=6.2831853071795860+00
      OMEGA = (RPM*TWOPI)/60.
      V=V*1.689
      MACH=V/CO
      G1=1.-MACH**2
      FREQO=OMEGA/TWOPI
      FNDFRQ= FREQO*M*NB
      AK = K/10.
      WVNMBR=TWOPI*FNDFRQ/CO
      DBETA = (TWOPI/360.) *DBETA
      PSI=(TWOPI/360.)*PSI
      GAMMA=GAMMA*PI/180.
      Q = Q/12.
      FQ = Q/(AK*R)
      CVFCTR= 4.45E+05/(2.54**2)
      FRCMAG=SQRT(T**2+FQ**2+FRAD**2)
      ALPHA= ATAN(FQ/T)
      PHIC=ATAN(FRAD/T)
      DELS=0.01 *((TWOPI*CO)/(M*NB*OMEGA))
      NSRCE = 2*NSOPLS
      DTHETA = TWOPI/NSOPLS
C     PRINT RUN CONSTANTS
      WRITE(6,DATUSE)
      THETAR=THETAR*TWOPI/360.
C     INITIALIZE ANSWER MATRIX
      DO 310 LL=1,NFP
  310 ANSTOT(2,LL)=0.
      IF(LOADLW.EQ.0.) GO TO 1108
C     COMPUTE MAGNITUDE OF LOADING HARMONICS IF LOADING LAW IS USED
      IF(NSTART.NE.1) GO TO 1102
      AHARM(1)=1.
      APHSE(1)=0.
      NSTRT=2
      WRITE(6,1150)
 1150 FORMAT(' LAMBDA=1',5X,'AHARM=1',5X,'APHSE=0.')
      GO TO 1101
 1102 NSTRT=NSTART
 1101 DO 1100 NN=NSTRT,NHARM
      AHARM(NN)=1./((NN   -1)**LOADLW)
```

```
      APHSE(NN)=0.
 1100 WRITE(6,1151)NN,AHARM(NN)
 1151 FORMAT(' LAMBDA=',I5,5X,'AHARM=',E10.3,5X,'APHSE=0.')
      GO TO 1109
C     READ & PRINTOUT RECORD OF AIRLD HARM DATA-NOTE NMBR=1 IS STEADY
C     LOADING COMPONENT
 1108 DO124 NN=NSTART,NHARM
      READ(5,108)NMBR,AHARM(NN),APHSE(NN)
  108 FORMAT(I5,5X,2E10.3)
      WRITE(6,150)NMBR,AHARM(NN),APHSE(NN)
  150 FORMAT(1H ,'NMBR=HARM+1=',I5,5X,'AHARM=',E10.3,'APHSE=',E10.3,'DEG
     1')
  124 APHSE(NN)=APHSE(NN)*TWOPI/360.
C     COMPUTE EQUIVALENT MONOPOLE SOURCE DISTRIBUTION FOR HORIZ ROTOR
 1109 DO 300 IHM=NSTART,NHARM
       NNM1=IHM-1
    7 DO 8 J=1,NSRCE,2
      MULT = 1
      KK = J
      THETA = -DTHETA + ((KK+1)/2)*DTHETA
      XXX=APHSE(IHM)
       FMAG=FRCMAG*AHARM(IHM)*(COS(NNM1*(THETA-THETAR)-XXX))
    9 SOURCE(1,KK) = AK*R*COS(THETA)+MULT*SIN(ALPHA)*SIN(THETA)*
     1(DELS/2.)-MULT*COS(THETA)*COS(ALPHA)*SIN(PHIC)*(DELS/2.)
      SOURCE(2,KK) = H+MULT*COS(ALPHA)*(DELS/2.)*COS(PHIC)
      SOURCE(3,KK) = -AK*R*SIN(THETA)+MULT*SIN(ALPHA)*COS(THETA)*
     1(DELS/2.) +MULT*SIN(THETA)*COS(ALPHA)*SIN(PHIC)*(DELS/2.)
      SOURCE(4,KK)=MULT*SRCMAG(FMAG,TWOPI,DELS,DTHETA)
      SOURCE(5,KK) = PHASE(THETA,OMEGA,AK,R,C,M,NB)
      IF(MULT.LT.0) GO TO 8
      MULT = -1
      KK = KK + 1
      GO TO 9
    8 CONTINUE
      IF(PSI.EQ.0.) GO TO 330
C     CORRECT SOURCE DISTRIBUTION FOR TILT ANGLE IF ROTOR NOT HORIZ
      DO 331 J=1,NSRCE
      XZRO=SOURCE(1,J)
      YZRO=SOURCE(2,J)
      SOURCE(1,J)=XZRO*COS(PSI)-(YZRO-H)*SIN(PSI)
  331 SOURCE(2,J)=XZRO*SIN(PSI)+(YZRO-H)*COS(PSI)+H
  330 IF(NPNCH.NE.1) GO TO 13
C     PUNCH EQIV ACOUSTIC SOURCE DATA CDS FOR CURRENT AIRLD HARM
   10 DO 11 J=1,NSRCE
      WRITE(7,12) (SOURCE(I,J),I=1,5)
   12 FORMAT(5E15.8)
   11 CONTINUE
      WRITE(7,212)
  212 FORMAT(80X)
   13 IF(NPRNT.NE.1) GO TO 18
C     PRINT EQUIV ACOUSTIC SOURCE DATA AS OUTPUT
      WRITE(6,16)
   14 DO 15 J=1,NSRCE
      WRITE(6,17) J,(SOURCE(I,J),I=1,5)
   16 FORMAT(1HO,'SOURCE CARDS DEVELOPED FOR EFFECTIVE RING APPROX TO PR
     1OPELLER ARE-'/1HO,'CARD',T16,'XI(FT)',T36,'YI(FT)',T56,'ZI(FT)',
     2T71,'MAGNITUDE(LB/SQFT)',T93,'PHASE(RADIANS)')
   17 FORMAT(1H ,I5,5(5X,E15.8))
   15 CONTINUE
   18 IF(NPLOT.NE.1) GOTO 24
```

```
C      PRINT DATA FOR POLAR PLOT OF ACOUSTIC FLD OF CURRENT AIRLD HARM
       WRITE(6,119) IHM
   19  DO 20 L = 1,NFP
       BETA = (L-1)*DBETA
       XR = RFP*COS(BETA)*COS(GAMMA)
       YR = H-RFP*SIN(BETA)
       ZR=RFP*COS(BETA)*SIN(GAMMA)
       REAL = 0.
       AIMAG = 0.
   21  DO 22 N=1,NSRCE
       XOPT=SOURCE(1,N)-XR
       RSQRD=(YR-SOURCE(2,N))**2+(ZR-SOURCE(3,N))**2
       DIST=(-MACH*XOPT+SQRT(XOPT**2+G1*RSQRD))/G1
       DIST2=DIST**2
       XE=XOPT-MACH*DIST
       E2=ABS(1.-RSQRD/DIST2)
  351  CSANGL= SIGN(SQRT(E2),XR-XE)
       DBLP=(M*NB*OMEGA)/CO
       ARG=SOURCE(5,N)-DBLP*DIST
       ARG=DMOD(ARG,TWOPI)
       F1=1.-MACH*CSANGL
       CORCTN=1.+(((CSANGL-MACH)*MACH)/(WVNMBR*DIST*F1))**2
       PS=0.
       IF(CORCTN.GT.0.) GO TO 350
       PS=PI/2.
       CORCTN=-CORCTN
  350  CORCTN=SQRT(CORCTN)/(F1**2)
       DIST1=DIST
       CORANG=ATAN(((MACH-CSANGL)*MACH)/(WVNMBR*DIST1*F1))
       CORANG=AMOD(CORANG,2.*PI)
       ARG=ARG+CORANG +PS
       REAL=REAL+ (SOURCE(4,N)*DCOS(ARG)*CORCTN)/DIST
   22  AIMAG=AIMAG+ (SOURCE(4,N)*DSIN(ARG)*CORCTN)/DIST
       SUMMAG =DSQRT(REAL**2+AIMAG**2)/(SQRT(2.))
       IF(AIMAG.NE.0.) GO TO 222
       IF(REAL.NE.0.) GO TO 222
       SMPHSE=0.
       GO TO 223
  222  SMPHSE= DATAN2(AIMAG,REAL)
  223  DEGBET = BETA*(360./TWOPI)
       DEGPS = SMPHSE*(360./TWOPI)
       AMPPSI=SUMMAG/144.
       ASQRD=AMPPSI**2
       IF(AMPPSI.NE.0.) GO TO 323
       AMPDB= -1.0E+10
       GO TO 23
  323  AMPDB= 20.*ALOG10(AMPPSI*CVFCTR)
   23  WRITE(6,122) L,RFP,DEGBET,SUMMAG,SMPHSE,DEGPS,AMPPSI,AMPDB,ASQRD
  122  FORMAT(1H ,I5,T11,E10.3,T26,E10.3,T41,E10.3,T56,E10.3,T71,E10.3,
      1T87,E10.3,T101,E10.3,T116,E10.3)
       ANSTOT(1,L)=DEGBET
       ANSTOT(2,L)=ANSTOT(2,L)+ASQRD
   20  CONTINUE
  300  CONTINUE
C      PRINTOUT POLAR PATTERN DATA DUE TO EFFECTS OF ALL AIRLD HARM USED
  119  FORMAT(1HO,'POLAR PATTERN DATA FOR LAMBDA =',I3,' FOLLOWS'
      1/1H ,'FLD PT',T11,'RADIUS (FT)',
      1      T26,'ANGLE(DEG)',T41,'AMPLITUDE',T56,'PHASE(RAD)',T71,'PHASE
      2(DEG)',T86,'AMPL(PSI)',T103,'A(DB 1UB)',T118,'A**2 PSI')
       WRITE(6,311)
```

```
  311 FORMAT(1HO,'POLAR PATTERN DATA FOR TOTAL PRESS DUE TO ALL AIRLD HA
     1RM FOLLOWS-'/1H ,'ANGLE(DEG)',T21,'TOT PRESS(PSI)',T41,'TOT PRESS(
     2DB RE 1 UB)')
      DO 312 LL=1,NFP
      ANSTOT(2,LL)=SQRT(ANSTOT(2,LL))
      ANSDB=20.*ALOG10(ANSTOT(2,LL)*CVFCTR)
  312 WRITE(6,313)ANSTOT(1,LL),ANSTOT(2,LL),ANSDB
  313 FORMAT(1H ,E10.3,T25,E10.3,T45,E10.3)
      GO TO 1
   24 WRITE(6,25)
   25 FORMAT(1HO,'PROGRAM COMPLETED-NORMAL EXIT')
      STOP
      END
C     THIS FUNCTION SUBPROGRAM COMPUTES THE PHASE OF ANY SOURCE LOCATED
C     ON THE PERIPHERY OF THE EFFECTIVE RING OF THE ROTOR.
      REAL FUNCTION PHASE*8(THETA,OMEGA,AK,R,C,M,NB)
      PHASE = -((THETA/OMEGA)+(C/(2.*OMEGA*AK*R)))*M*NB*OMEGA
      RETURN
      END
C     THIS FUNCTION SUBPROGRAM COMPUTES THE MAGNITUDE OF THE FOURIER
C     COMPONENTS OF THE SERIES EXPANSION OF THE FORCE-TIME CURVE
C     RELATING TO THE EFFECTIVE RING APPROX TO THE ROTOR NOISE FIELD
C     THIS VERSION ASSUMES AN IMPULSIVE PRESSURE-TIME HISTORY
      REAL FUNCTION SRCMAG*8(FRCMAG,TWOPI,DELS,DTHETA)
      REAL*8 TWOPI
      SRCMAG= (FRCMAG/(TWOPI**2*DELS))*DTHETA
      RETURN
      END
/*          THIS IS A SLASH ASTERISK CARD
```

References

1. C. M. Harris, Handbook of Noise Control, McGraw-Hill, 1957.

2. L. Gutin, On the Sound Field of a Rotating Propeller, NACA Technical Memorandum 1195, 1948 (translation).

3. I. E. Garrick and C. E. Watkins, A Theoretical Study of the Effect of Forward Speed on the Free-Space Sound-Pressure Field Around Propellers, NACA Report 1198, 1954.

4. R. Schlegel, R. King, and H. Mull, Helicopter Rotor Noise Generation and Propagation, USAAV Labs Technical Report 66-4, 1965 (also available from the Defense Documentation Center as AD 645-884).

5. R. Schlegel and W. E. Bausch, "Helicopter Rotor Noise Prediction and Control," Journal of the American Helicopter Society, July 1961 pp. 38-47.

6. M. V. Lowson, "The Sound Field for Singularities in Motion," Proceedings of the Royal Society of London, A Vol. 286, August 1965, pp. 559-572.

7. M. V. Lowson and J. B. Ollerhead, Studies of Helicopter Rotor Noise, Wyle Research Staff Report WR 68-9, USAAVLABS Technical Report 68-60, Fort Eustis, Virginia, January 1969. (Note, this report is summarized in M. V. Lowson and J. B. Ollerhead, Problems of Helicopter Noise Estimation and Reduction, AIAA Paper No. 69-195, AIAA/AHS VTOL Research, Design, and Operations Meeting, Georgia Institute of Technology, Atlanta, Georgia, February 17-19, 1969.)

8. M. J. Lighthill, "On Sound Generated Aerodynamically," Part 1: General Theory, Proceedings of the Royal Society of London, A Vol. 211, 1952, pp. 564-587.

9. L. E. Kinsler and A. R. Fry, Fundamentals of Acoustics, Wiley, 1962.

10. J. Scheiman, A Tabulation of Helicopter Rotor-Blade Differential Pressures, Stresses and Motions, as Measured in Flight, NASA TM-X-952, Washington, D. C., March 1964.

11. F. B. Burpo and R. R. Lynn, Measurement of Dynamic Airloads on a Full-Scale Semi-Rigid Rotor, Bell Helicopter Co., TCREC Technical Report 62-42, U. S. Army Transportation Research Command, Fort Eustis, Virginia, 1962.

12. P. M. Morse and K. V. Ingard, Theoretical Acoustics, McGraw-Hill Book Co., First Edition, 1968.

13. T. J. Stuckey and J. O. Goddard, "Investigation and Prediction of Helicopter Rotor Noise; Part 1. Wessex Whirl Tower Results," Journal of Sound and Vibration, Vol. 5, No. 1, January 1967, pp. 50-80.